Macromolecules
ARTICLE

Macromolecules **2010**, *43*, 3511–3520 **3511**
DOI: 10.1021/ma9027273

Colloids in Brushes: The Insertion Free Energy via Monte Carlo Simulation with Umbrella Sampling

V. Ermilov and A. Lazutin

A. N. Nesmeyanov Institute of Organoelement Compounds, Russian Academy of Sciences, Vavilova str. 28, 119991, Moscow, Russia

A. Halperin*

Laboratoire de Spectrométrie Physique (UMR 5588), Université Joseph Fourier—CNRS, BP 87, 38402 Saint Martin d'Hères, France

Received December 14, 2009; Revised Manuscript Received February 18, 2010

ABSTRACT: The insertion of spherical, nonadsorbing colloidal particles into a swollen planar polymer brush is characterized using Monte Carlo simulations with umbrella sampling focusing on small particles whose radius R_p is smaller than the unperturbed brush thickness, h_0. This process plays a key role in the modeling antifouling poly(ethylene glycol) brushes that repress protein adsorption. Two properties are studied as a function of R_p and the altitude within the brush z: (i) The particle induced perturbation of the monomer concentration profile and (ii) The insertion free energy penalty, F_{ins}. The perturbation of the concentration profile is short ranged involving pure depletion at high z and depletion followed by a maximum at low z. When the particle does not experience the surface depletion layer F_{ins} grows with the monomer volume fraction ϕ and R_p. $F_{ins} \sim R_p^3$ for the larger R_p reflects an osmotic insertion penalty at the high ϕ range of the brush. At the lower ϕ range a surface tension correction plays a role. In the range explored there is no evidence for $F_{ins} \sim R_p^{4/3}$ as was suggested for small particles.

I. Introduction

The free energy penalty incurred upon introducing colloids into a polymer brush attracted attention from two perspective. One concerned melt brushes having in mind the design of colloid−polymer composite materials.[1,2] The second involves swollen brushes of neutral water-soluble polymers (NWSP) as utilized to tune surface interactions with proteins in aqueous media.[3−8] Two examples illustrate this last category. First, brushes of poly(ethylene glycol) (PEG) displayed to repress nonspecific protein adsorption.[9−13] Second, brushes of temperature responsive polymers such as poly(*N*-isopropylacrylamide) (PNIPAM) enabling to switch protein adsorption by a small change of temperature. In particular, PNIPAM brushes are of use in harvesting cell sheets as well as in protein chromatography.[14,15] Importantly, surfaces displaying NWSP, and PEG in particular, are used to prolong the blood circulation time of protein drugs[16] and drug bearing liposomes.[17] Our work is motivated by the second direction, having in mind primarily the repression of protein adsorption. The scope of this problem is wide even if one limits the discussion to PEG brushes. It involves an interplay of different attraction free energies favoring adsorption with an insertion penalty that opposes it. The attraction free energies vary with the identity of the adsorbing proteins and the nature of the surface. They may reflect contributions from surface−protein contact attraction,[3−6] long ranged van der Waals attraction between the surface and the protein,[3−5] weak *nonspecific* attraction between the protein and the polymer[6,8] or strong *specific* protein−polymer attractions.[18] In contrast, the insertion penalty, F_{ins}, is roughly independent of the detailed characteristics of the system. For an approximately spherical protein of radius R_p its form is largely determined by the ratio of R_p/h_0 where h_0 is the height of the unperturbed brush[5,7] (Figure 1). When $R_p \gg h_0$ the particle can only approach the surface by compressing the brush.[3] In this "compressive" case F_{ins} is traceable to the increased monomer concentration in the compressed brush. In the opposite limit, when $R_p \ll h_0$,[4−6,8] the protein perturbs the brush structure only locally and F_{ins} of the "insertive" case is related to the penalty of inserting the particle into a semidilute solution of free polymers.

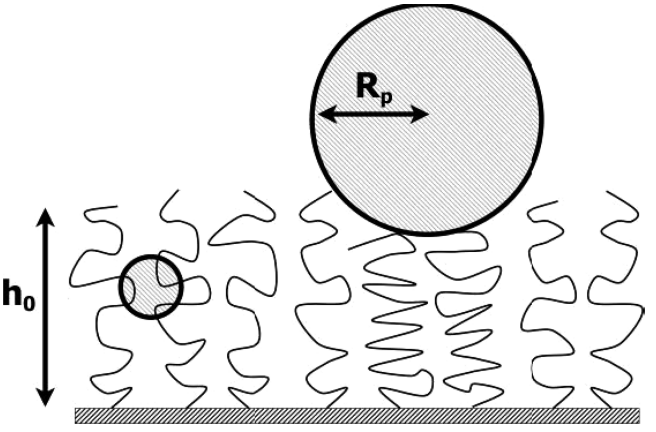

Figure 1. Compressive vs insertive modes: large particles can only approach the surface by compressing the brush while the insertion of small particles gives rise only to a local perturbation.

Our off-lattice Monte Carlo simulations aim to characterize F_{ins} of the insertive case as realized for spherical, nonadsorbing

*Corresponding author. E-mail: avraham.halperin@ujf-grenoble.fr.

© 2010 American Chemical Society

Published on Web 03/10/2010

and rigid particles. These particles serve as simplified models of dense globular proteins whose insertion penalty is largely determined by their excluded volume. In particular we address three issues: (a) The particle induced perturbation of the monomer concentration profile and its range. (b) The variation of F_{ins} with the altitude z and the particle radius R_p. (c) The relationship between F_{ins} and the corresponding insertion free energies in solutions of free polymers when R_p is larger or smaller than the blob size ξ, i.e., $R_p > \xi$ or $R_p < \xi$. To investigate this last point we compare the brush $F_{ins}(z)$, as obtained from the simulation, to the theoretical F_{ins} in a bulk solution with monomer volume fraction ϕ corresponding to $\phi(z)$ of the unperturbed brush. We focus on the simplest case involving impenetrable rigid spheres and a monodispersed brush of flexible chains swollen by an athermal solvent. In this form the simulation and the analysis are relatively straightforward because both monomers and the particle are modeled as hard-core spheres. To obtain F_{ins} we utilize umbrella sampling and introduce a simple method of obtaining F_{ins} from the measured equilibrium altitude of the inserted particle in the brush. Our results suggest that the particle induces a local perturbation of the ϕ profile. The decay length is comparable to the monomer diameter a. In particular, the ϕ profile around the particle attains its unperturbed value within a distance of roughly $\approx 2a$ to $\approx 6a$ depending on the altitude z. The associated F_{ins} increases with R_p and $\phi(z)$. Accordingly, F_{ins} increases with the penetration depth until it reaches the vicinity of the wall where the effect of the depletion layer at the grafting surface is evident. F_{ins} of the larger particles at high $\phi(z)$ is proportional to the osmotic penalty incurred upon introducing a particle of volume V_p into a brush with a local osmotic pressure $\Pi(z) \approx kT/\xi(z)^3$, $F_{ins} \approx \Pi(z)V_p \approx (R_p/\xi)^3$, as was conjectured previously.[5,8,18] Interestingly plots of $F_{ins}/{R_p}^3$ also collapse the data of large particles at small $\phi(z)$ where the applicability of $F_{ins} \approx \Pi(z)V_p$ is not evident. For the range of R_p explored we find no evidence for the $R_p \ll \xi$ limit, where $F_{ins}/kT \approx (R/\xi)^{4/3}$, even for particles such that $R_p < \xi(z)$ holds for all altitudes z. However, in the low ϕ region there are indications for surface tension corrections of the form $(R_p/\xi)^2$.

The assumptions underlying our work are also invoked by a number of theories concerning brush-protein interactions.[4−8,18] Our results are thus relevant to the discussion and the modeling of these systems. In addition, the results concerning F_{ins} in brushes, and the methodology used to obtain them, are of interest for the polymer physics of solutions and surface layers. Two prior simulation studies investigated related systems. An early simulation by Jönsson and Johansson characterized F_{ins} utilizing a lattice model in combination with the Widom insertion method.[19] More recently Milchev et al. studied F_{ins} using an off-lattice model with Morse interaction potentials and the "particle inflation method", a generalization of the Widom insertion method.[2] Complete confrontation with these studies is not straightforward because of differences between the polymer models utilized, the brush densities considered and the methods used to obtain F_{ins}. Our analysis is also somewhat different in that it aims to compare the measured F_{ins} to theoretical results concerning F_{ins} in semidilute solutions. We return to this issue in sections IV and V.

A summary of the relevant theory concerning the insertion free energy penalty in bulk solutions and brush structure is presented in section II. It motivates the questions addressed in this paper as well as the analysis of the data. The simulation of the brush as well as the umbrella sampling method utilized to obtain F_{ins} are described in section III. Here we also discuss the comparison between three different methods of obtaining F_{ins} and their performance. The simulation results concerning the concentration profiles and $F_{ins}(z, R_p)$ are presented in section IV. It also contains plots confronting the measured $F_{ins}(z, R_p)$ and the theoretical expressions discussed in section II. An overall view of our results is presented in section V.

II. The Insertion Penalty: General Considerations

The goal of this work is to confront simulation results with a simple analytical description of the "insertive" case, $R_p \ll h_0$. In particular, it aims to test the following two assumptions: (i) the inserted particle induces a local, short ranged, perturbation of the brush structure (ii) the associated penalty at altitude z is related to F_{ins} into a uniform polymer solution with $\phi = \phi(z)$ of the unperturbed brush. With this in mind, we first summarize the necessary background concerning F_{ins} for solutions of free polymers, brush structure as well as some general consideration regarding the insertion penalty in a brush.

F_{ins} of a large, spherical and nonadsorbing particle into a polymer solution with a uniform ϕ reflects two contributions: $F_{ins} = \Pi(\phi)V_p + \gamma(\phi)A_p$.[20] Here $\Pi(\phi)$ is the osmotic pressure of a solution and $\Pi(\phi)V_p$ is the osmotic work expended upon insertion of a particle of volume $V_p \approx {R_p}^3$. $\gamma(\phi)$ is the surface tension due to the depletion layer surrounding the particle, $\gamma(\phi)A_p$ is the work associated with its creation and the particle surface area is $A_p \approx {R_p}^2$. In a good solvent both $\Pi(\phi)$ and $\gamma(\phi)$ are determined by the blob size $\xi \approx a\phi^{-3/4}$,[21,22] with $\Pi(\phi) \approx kT/\xi^3$[21,22] and $\gamma(\phi) \approx kT/\xi^2$,[23] where k is the Boltzmann constant and T is the temperature. Accordingly, F_{ins} of a spherical particle, neglecting numerical prefactors, is

$$F_{ins}/kT \approx (R_p/\xi)^3 + (R_p/\xi)^2 = (R_p/\xi)^3[1 + (\xi/R_p)] \quad (1)$$

and for $R_p \gg \xi$ it is well approximated by

$$F_{ins}/kT \approx \Pi(\phi)V_p/kT \approx (R_p/\xi)^3 \quad (2)$$

or kT per blob displaced by the particle. In the opposite limit of $R_p \ll \xi$[23−26]

$$F_{ins}/kT \approx (R_p/\xi)^{4/3} \quad (3)$$

and the resulting F_{ins} is higher than the corresponding $(R_p/\xi)^3$. Eq 3 can be rationalized, following Sear,[27] noting that a particle of radius R_p experiences excluded volume interactions with chain segments of span $\sim R_p$ comprising $g_{R_p} \approx (R_p/a)^{5/3}$ monomers. A blob consisting of $g \approx (\xi/a)^{5/3}$ monomers contains $n_{R_p} \approx g/g_{R_p} \approx (\xi/R_p)^{5/3}$ such segments. The excluded volume to particle insertion within a blob of volume ξ^3 is thus $n_{R_p}{R_p}^3$. The probability of successful insertion of a particle into the blob, without incurring chain-particle overlap, is $p_{ins} = 1 - p_{ov} \approx 1 - (R_p/\xi)^{4/3}$ where $p_{ov} \approx n_{R_p}{R_p}^3/\xi^3$ is the probability of a failed insertion due to an encounter with a chain segment. In turn, this determines the insertion free energy within the Widom method $F_{ins}/kT \approx -\ln p_{ins} \approx (R_p/\xi)^{4/3}$. The existence of the two F_{ins} forms reflects thus the degree of uniformity of the polymer solution as probed by the particle. In the $R_p \gg \xi$ limit, the inserted particle experiences an effectively uniform environment, while in the $R_p \ll \xi$ limit, it encounters a heterogeneous medium comprising "forbidden" regions occupied by the chain as well as "allowed" regions consisting of pure solvent.

The range of applicability of $\Pi(\phi)V_p/kT \approx (R_p/\xi)^3$ is limited to the semidilute regime. A useful extrapolation form for $\Pi(\phi)$, with a wider applicability range, was proposed by Fleer et al.[28] For athermal solvent, it assumes the form

$$\frac{\Pi(\phi)a^3}{kT} = \frac{\phi}{N}\left[1 + \left(\frac{\phi}{\phi_{ex}}\right)^{1.309}\right] \quad (4)$$

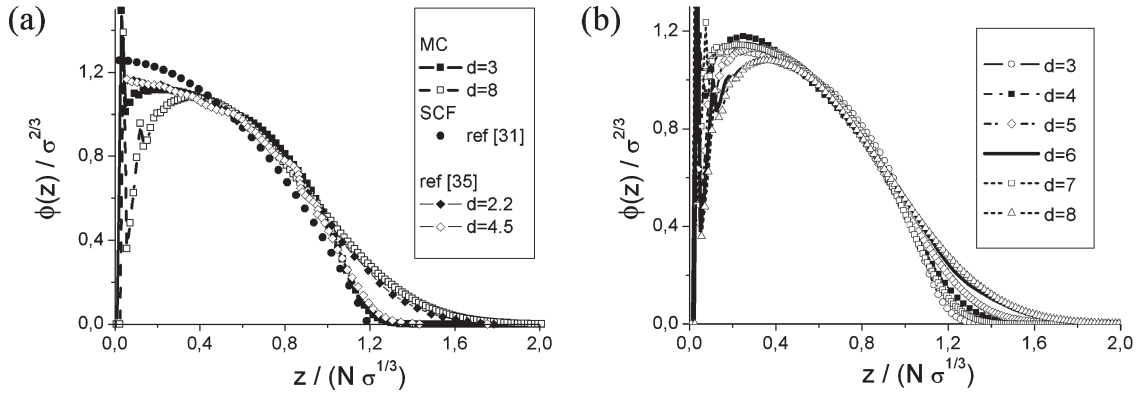

Figure 2. Reduced concentration $\phi/\sigma^{2/3}$ vs the reduced height $z/N\sigma^{1/3}$ for (a) unperturbed brushes as obtained in our simulations for different d values and (b) as compared to simulation results of[37,41] and $\phi(z)$ given by SCF theory for marginal solvent[33,36] for $d = 3$ and $d = 8$.

where $\phi_{ex} = A\phi^*$ is an "extrapolation concentration" related to the overlap threshold

$$\phi^* = \frac{3}{4\pi}\frac{Na^3}{{R_F}^3} \sim N^{1-3v}$$

where v is the Flory exponent. For an athermal solvent Fleer et al proposed $A = 0.69$ upon fitting eq 4 to a renormalization group expression due to Schaefer[29]

$$\frac{\Pi(\phi)a^3}{kT} = \frac{\phi}{N}\left[1 + 1.314\left(\frac{1 + 2.4167\bar{\phi} + 0.9956\bar{\phi}^2}{1 + 0.5099\bar{\phi}}\right)^{0.309}\right] \quad (5)$$

where $\bar{\phi} = \phi/\phi^*$. Importantly, this form applies to the $N \to \infty$ limit when $\Pi(\phi)a^3N/kT\phi = f(\bar{\phi})$ is a universal function. For finite N it is necessary to account for scaling corrections[30] and the universal $f(\bar{\phi})$ is multiplied by a factor $[1+k_z g(\bar{\phi})/N^{\Delta}]$ where k_z is a system specific constant, $\Delta = 0.515$ and $g(\phi)$ is a universal function scaling as $g(\bar{\phi}) \sim \bar{\phi}^{0.675}$ for large $\bar{\phi}$. As we shall see eq 4 will prove useful in the discussing the qualitative features of F_{ins}. However, the applicability of $A = 0.69$ to our system is not evident because the chains in our simulations are short, $N = 50$, and scaling corrections may be significant.

The preceding discussion of F_{ins} requires adaptation when the particle is inserted into a brush rather than into a bulk polymer solution. It is first helpful to distinguish two modes[5,7,8] of approaching the grafting surface, depending on the ratio of R_p and the unperturbed brush height h_0. Large particles with $R_p \gg h_0$ can only approach the surface by compressing the brush.[3,5] In the opposite limit $R_p \ll h_0$ one expects that the brush structure will be perturbed only within a narrow region surrounding the particle.[4,5,7] In the following we focus on this second, "insertive" regime. Our discussion concerns the simplest approach to the insertive case, invoking the bulk solution form of F_{ins}. However, these results concern polymer solutions of uniform concentration comprising undeformed chains in the absence of an impenetrable surface. In contrast, the brush comprises stretched chains attached to an impenetrable surface and its concentration profile varies with the altitude z, along the normal to the grafting surface. To discuss the implications of these differences it is first helpful to recall the leading features of the brush structure.

The self-consistent field (SCF) of brushes in marginal solvents[31−33] yields a parabolic monomer concentration profile

$$c(z) = c_0(1 - z^2/h_0^2) \quad (6)$$

where the volume fraction at the grafting surface $z = 0$, $\phi_0 = c_0a^3$ is

$$\phi_0 = \frac{3}{2}\left(\frac{\pi^2a^3}{8p\mathrm{v}}\right)^{1/3}\left(\frac{a^2}{\Sigma}\right)^{2/3} \quad (7)$$

and the height of an unperturbed brush is

$$\frac{h_0}{a} = \left(\frac{8}{\pi^2}\right)^{1/3} N\left(\frac{p\mathrm{v}}{a^3}\right)^{1/3}\left(\frac{a^2}{\Sigma}\right)^{1/3} \quad (8)$$

Here p is the number of monomers in a persistence length, v is the second virial coefficient of monomer−monomer interactions, $\mathrm{v} \approx a^3\tau$ where $\tau = 1 - \Theta/T$, a is the monomer diameter, Θ is the theta temperature, and Σ is the area per chain. While the parabolic profile is derived for marginal solvent, the profile obtained for athermal solvent is very similar.[34,35] The observed $\phi(z)$ in athermal solvent (Figure 2) is in reasonable agreement with eqs 6−8 with $p = 1$ and a second virial coefficient of a hard-core sphere fluid of monomers, $\mathrm{v} = 2\pi a^3/3$.[36] Importantly, the SCF results apply to brushes of long chains and high grafting densities ignoring short-range surface effects. Simulation studies of brush structure reveal two deviations from the SCF results,[33,34,37] both are relevant to our subsequent discussion. First, a depletion layer occurs at the grafting surface. It is associated with a rapidly decaying oscillations in the concentration profile. For semidilute brushes $\phi(z)$ exhibits a maximum at z_{max} located within a distance of few a from the surface. Second, finite size brushes exhibit an exterior edge where the strong stretching assumption is not fulfilled and concentration fluctuations play a role. In this outer edge, whose span can reach 10−20% of the brush height, the chains are reminiscent of bulk semidilute solution at the vicinity of the overlap threshold. The exterior region also displays a weak non parabolic tail.[34]

With these observations in mind, the simplest estimate of F_{ins} incurred upon insertion of a single particle at altitude z in the brush is F_{ins} of insertion into a uniform bulk solution with $\phi = \phi(z)$ corresponding to the position of the center of the particle. This estimate is very rough because the brush F_{ins} is traceable to both monomer−monomer interactions and the stretched configurations of the chains.[35] As noted earlier, this rough approximation is reasonable only when the insertion of particle results in short-range modification of the brush concentration profile. When $R_p \ll h_0$ this estimate also benefits from the small variation of the parabolic $\phi(z)$, as given by eq 6, over a distance R_p. Its performance is further enhanced because the sphere's volume

elements closer to the grafting surface experiences higher $\phi(z)$ than the "outer" volume elements and the associated errors partially cancel. Note that the compressive and insertive regimes occur also for nonspherical particles but the regime boundaries require a more elaborate analysis. For example, for disk-like particles it is necessary to distinguish between edgewise insertion and insertion with the disk surface parallel to the grafting surface. For simplicity we confine our analysis to spherical particles with $R_p \ll h_0$. Clearly, our discussion of insertive regime applies only when particle−particle interactions within the brush can be neglected. This is certainly the case for our simulations which concern the insertion of a single particle. This "dilute brush" regime is also of practical interest since the design of antifouling brushes involves tuning of the adsorption threshold, when the insertion penalty largely represses protein adsorption.

Note that the concentration profile of the brush implies that different F_{ins} may apply at different altitudes. For example, the crossover between $F_{in}/kT \approx (R_p/\xi)^{4/3}$ and the $F_{in}/kT \approx \Pi(\phi)V_p/kT \approx (R_p/\xi)^3$ regimes occurs around $\xi \approx R_p$. Since $\xi \approx a\phi^{-3/4}$, this suggests a boundary at roughly

$$\phi_{osm} \approx (a/R_p)^{4/3} \tag{9}$$

such that the osmotic penalty is operative in brush regions with $\phi > \phi_{osm}$ while the de Gennes penalty occurs at lower ϕ.

III. Simulation Method

In our Monte Carlo simulation spherical impenetrable particles of radius R_p are introduced into a planar brush of monodispersed chains comprising N monomers of diameter a. All lengths will be expressed in units of a. The immobile grafting sites form an array of $n \times n$ sites on square lattice with an edge length d at the $x - y$ surface of the simulation box. The brush thus extends in the z direction. The simulation box dimensions are $l_x \times l_y \times l_z$ with $l_x = l_y = nd$, and $l_z = 1.2 \times N$. l_z corresponds to a fully extended polymer to avoid restrictions of the chains' configurations. Periodic boundary condition apply in the x and y directions while the surfaces at $z = 0$ and $z = l_z$ are impenetrable.

Most of our simulations concerning free energy determination utilize $N = 50$, $n = 10$ and $d = 3$ leading to simulation box with $l_x = l_y = 30$, $l_z = 60$ and 100 grafted chains with grafting density $\sigma = 1/d^2 \approx 0.111$. To verify the quality of the brush simulations we also simulated brushes with $4 \le d \le 8$ with corresponding larger simulation boxes and with grafting densities $\sigma \simeq 0.063$, 0.040, 0.028, 0.020, and 0.016. We confirmed that the simulation of brushes involving the largest inserted particles, $R_p = 5$, yielded identical concentration profiles around the particles for both $n = 20$ and for $n = 10$. This in turn suggests that the perturbation range is independent of the size of the simulation box.

The polymers are modeled as freely jointed chains of spherical hard-core monomers of radius $r = 0.5$. Chain connectivity is imposed by a square-well potential between adjacent monomers along the chain[38]

$$U_{\text{chain}}(r_{i,i+1}) = \begin{cases} 0, & 1 < r_{i,i+1} < 1.2 \\ \infty, & r_{i,i+1} \notin (1, 1.2) \end{cases} \tag{10}$$

where $r_{i,i+1}$ is the distance between the centers of monomer i and its immediate neighbor along the chain $i + 1$. Accordingly the bond length fluctuates freely between 1, when the two monomers are in grazing contact, and 1.2. Binary interactions between monomers i and j reflect pure hard-core repulsion

$$U_{\text{ex}}(r_{ij}) = \begin{cases} 0, & r_{ij} > 2r = 1 \\ \infty, & r_{ij} \le 2r = 1 \end{cases} \tag{11}$$

where r_{ij} is distance between the centers of monomers i and j. The choice of a maximal $r_{i,i+1} < \sqrt{2}$ thus prevents phantom chain behavior, chain crossing, as this incurs $U_{\text{ex}} = \infty$. The inserted particle is modeled as an impenetrable sphere of radius $0.5 \le R_p \le 5$ interacting with a monomer of radius $r = {}^1/_2$ via

$$U_{\text{mp}}(r_{pj}) = \begin{cases} 0, & r_{pj} > r + R_p \\ \infty, & r_{pj} \le r + R_p \end{cases} \tag{12}$$

where r_{pj} is the distance between the centers of the particle and of monomer j.

We first describe the Monte Carlo simulation of the "bare" brush and then discuss the insertion of the particle. A monomer is chosen at random. For each monomer chosen, a trial move comprises of three independent random displacements along the x, y, and z axes. Since the monomers interact as hard spheres the energy change associated with each trial, ΔU, can assume only two values: $\Delta U = 0$ or $\Delta U = \infty$, depending on whether the move resulted in monomer overlap or not. Moves with $\Delta U = 0$ are accepted while moves with $\Delta U = \infty$ are rejected.[39,40] The initial configurations of the chains are fully stretched along the normal to the surface. The brush is equilibrated during 2×10^7 Monte Carlo steps (MCS) per monomer. After this equilibration period its concentration profile attained a stationary state. To further test the equilibration of the brushes we compared our results with earlier simulation results of Lai and Binder[37,41] as well as with SCF results for a marginal solvent[33,36] (Figure 2). The equilibrated brush configurations are then used as initial configuration for simulations aimed at particle insertion and the associated F_{ins}.

To obtain the insertion free energy of the particle, F_{ins} we utilize three methods summarized below: The Widom insertion method[42,43] and two versions of umbrella sampling.[43−45] In the one we named "force integration" we extract the F_{ins} from the equilibrium position of the particle. The other utilizes the self-consistent histogram (SCH) method.[43,46]

The Widom Insertion Method. Within the Widom insertion method[42,43] the excess chemical potential of insertion is obtained using the following procedure: (i) An insertion site is chosen at random. (ii) The associated insertion energy ΔU is calculated. Since only hard-core potentials are involved $\Delta U = 0$ if the particle does not overlap with a monomer and $\Delta U = \infty$ if it does. (iii) Following s trial insertions, we calculate the average of $\exp(-\Delta U/kT)$ over the ensemble of configurations of the particle-free brush, $\langle \exp(-\Delta U/kT) \rangle$. [47] Since

$$\exp(-\Delta U/kT) = \begin{cases} 0, \text{ particle−monomer overlap} \\ 1, \text{ no overlap} \end{cases} \tag{13}$$

the probability of a successful insertion of the particle, without incurring overlap with any of the monomers or bonds, is $p_{ins} = \langle \exp(-\Delta U/kT) \rangle$, i.e., $p_{ins} = m/s$ where m is the number of "successful insertions". Note that the procedure involves only trial insertions and the inserted particles are not retained within the brush. As the insertion penalty varies with the altitude z we calculate $p_{ins}(z)$ for bins of width Δz and the insertion penalty is specified by

$$F_{ins}(z) = -kT \ln p_{ins}(z) \tag{14}$$

Within our simulation $\Delta z = 0.5$ and the number of insertion attempts per bin and per configuration was $N_{ins} = 5$. Brush configuration were typically generated for 50×10^6 MCS and insertions were attempted at intervals of 100 MCS. Increasing the number of MCS to 240×10^6 did not affect the results.

The Widom method allowed to obtain F_{ins} for insertion of particles of $0.5 \leq R_p \leq 2.0$ into brushes with $N = 50$, $n = 10$ and $d = 3$. For $R_p = 3$ the number of successful insertion diminished rapidly with the insertion depth and no successful insertions were observed below $z = 20$ even in long simulations involving 240×10^6 MCS. Accordingly, we have utilized the Widom method only to obtain F_{ins} of small particles having $R_p \leq 2$.

Umbrella Sampling. The acceptance fraction of large particles within the Widom insertion method is very low and the associated poor statistics render this approach impractical for $R_p > 2$. An alternative approach suggests itself upon noting that the brush $F_{ins}(z)$ constitutes a potential barrier to particle-surface contact and the associated reaction coordinate is the altitude z. To improve the sampling statistics within the brush potential barrier we thus utilize Umbrella sampling[43−45] with harmonic bias potentials

$$W_i(z) = kT\kappa(z - z_{0i})^2 \tag{15}$$

These restrain the position of the particle to the vicinity of the minimum z_{0i} where κ is the force constant of the "harmonic spring". The sampled region is varied by tuning z_{0i}. The overall free energy experienced by a restrained particle at altitude z is thus

$$F_i(z) = F_{ins}(z) + W_i(z) \tag{16}$$

κ is chosen so that $F_{ins}(z_{0i})$ is comparable to $W_i(z_{0i})$ thus ensuring that the equilibrium position of the particle is affected by $F_{ins}(z)$. For $\kappa \gg 1$ the particle is sharply localized while for $\kappa \ll 1$ it essentially unconstrained. Accordingly we utilized a R_p dependent $\kappa(R_p) \lesssim 1$ as will be explained shortly. Before detailing the procedure note that, based on the bulk results summarized in section II, we expect $F_{ins}(z) = F_{ins}(\phi(z))$ to increase with $\phi(z)$. n particular F_{ins} should scale, depending on $R_p/\xi(z)$, either as $\phi^{9/4}$ or as ϕ. On the other hand, $\phi(z)$ of the unperturbed brush exhibits a maximum at z_{max} and $F_{ins}(\phi(z))$ should decrease with z for $z > z_{max}$. Accordingly, $F_i(z)$ can exhibit, in general, two minima and the outer one is dominant when $z_{0i} > z_{max}$.

To obtain $F_{ins}(z)$ of particles with $R_p > 2$, we performed several simulations utilizing different W_i with varying z_{0i}. The equilibration involved two processes. The first, using $\kappa = 100$ and a short 10^4 MCS relaxation, was used to create the initial configurations at each z_{0i}. During the $\kappa = 100$ processes the particles are strongly localized at z_{0i} and the equilibration affects mostly the chain configurations. Within this stage the particles were first restrained to $z_{0i} = 50$, outside an equilibrated "bare" brush, where $\phi(z_{0i}) = 0$. This equilibrated configuration was than used as initial configuration for the inserted particle at outer edge of the brush, $z_{0i} \simeq 35$. The equilibrated configuration obtained after 10^4 MCS was used as initial configuration for the next z_{0i} etc. After the creation of a full set of such "$\kappa = 100$ configurations", each with a different z_{0i}, the force constant was lowered to $\kappa \lesssim 1$ and the "$\kappa = 100$ configurations" were relaxed during $10-20 \times 10^6$ MCS. Within these processes the equilibration involves both the configurations of the chains and the altitude of the particle. The $\kappa \lesssim 1$ processes were implemented in two stages. The first was devoted to determining the restraining force constants $\kappa(R_p) \lesssim 1$ for each R_p explored using a procedure outlined later. In the second stage z-histograms $H_i(z)$ for each R_p and $\kappa(R_p)$ were acquired for every z_{0i} at intervals of 100 MCS for up to 50×10^6 MCS. The measured z histograms $H_i(z)$ specify the number configurations where the particle was localized at intervals between z and $z+\Delta z$. $H_i(z)$ determines the estimated biased probability distribution $p_i^{est}(z)$ for a finite sample

$$p_i^{est}(z)\Delta z = \langle H_i(z)\rangle / M \tag{17}$$

where M_i is number of points in histogram and $\langle ... \rangle$ denotes ensemble average. The set of z_{0i} was chosen so as to ensure both overlap between the resulting histograms and coverage of the range $z_{max} \geq z \geq h_0$. The equilibration period ensured $H(z) \gg 1$. The implementation of these criteria led to steps of $z_{0i} - z_{0i-1} = 3$ while the choice of the innermost z_{0i} varied with R_p. For $4 \leq R_p \leq 5.5$ we utilized $4 \leq z_{0i} \leq 35$ while for $0.5 \leq R_p \leq 3$ the explored range was $3 \leq z_{0i} \leq 33$. The procedure utilized for the determination of the $\kappa(R_p) \lesssim 1$ is a slight modification of the procedure described above. A full set of $\kappa = 100$ configurations was created for each R_p and in the last one the particle was placed in grazing contact with the surface i.e., $z_0 = R_p$. Within this stage only the $\kappa = 100$ configurations with $z_0 = R_p$ were relaxed further with the aim of probing the variation of $\langle z\rangle - z_0$ with κ. To choose $\kappa(R_p)$ we required $0 \ll \langle z\rangle - z_0 \ll h_0$ corresponding, for our paramters, to $2 < \langle z\rangle - z_0 < 4$. This procedure was implemented beginning with the smallest particle, $R_p = 3$, and then proceeding to the closest larger R_p and so on. For $R_p = 3$ we explored 12 κ values in the interval $10^{-4} \leq \kappa \leq 3$ each relaxed for 50×10^6 MCS and chose $\kappa(R_p = 3) = 0.2$ corresponding to $\langle z\rangle - z_0 \approx 2$. We than determined the $\kappa(R_p)$ of larger particles, in order of growing R_p, utilizing in each case an initial κ corresponding to the previous $\kappa(R_p)+0.1$. This value was retained if the relaxation lead to $2 < \langle z\rangle - z_0 < 4$ and otherwise κ was increased in increments of 0.1 until the condition $2 < \langle z\rangle - z_0 < 4$ was satisfied. Typically two iterations were required to obtain a $\kappa(R_p)$ leading altogether to the values: $\kappa(R_p = 3) = 0.2$, $\kappa(R_p = 4) = 0.4$, $\kappa(R_p = 4.5) = 0.6$, $\kappa(R_p = 5) = 0.9$.

Force Integration. In the range $z_{0i} > z_{max}$, where $\phi(z)$ is monotonically decreasing with z, the equilibrium position of the restrained particle, $z_{eq}(i)$ is specified by $\partial F_i(z)/\partial z = 0$, leading to

$$f[z_{eq}(i)] = \left.\frac{\partial F_{ins}(z)}{\partial z}\right|_{z=z_{eq}(i)} = 2\kappa k T[z_{eq}(i) - z_{0i}] \tag{18}$$

Here $f[z_{eq}(i)]$ is the outward directed force due to the interaction with the brush. Identifying $z_{eq}(i)$ with the measured average position in the ensemble obtained with the bias potential $W_i(z)$, $z_{eq}(i) = \langle z\rangle_i$, specifies the corresponding $f[z_{eq}(i)]$. Consequently the insertion free energy is obtained from

$$F_{ins}(z) - F_{ins}(\infty) = \int_{\infty}^{z} \mathrm{d}z_{eq}\,(i) f[z_{eq}(i)]$$

In practice, $z_{eq}(i) = \infty$ is replaced by $l_z \gg z > h_0$, where $\phi = 0$ and thus $F_{ins}(z) = 0$. Within this method $\langle z\rangle_i$ is obtained by averaging the z values of the particle at intervals of 100 MCS.

Self-Consistent Histogram Method. In the self-consistent histogram (SCH) [43,46] method $p(z)$ of the particle in the brush is constructed from a set of n z-histograms obtained for different bias potentials. The method is based on the assumption that the measured z histograms follow a Poisson distribution, with a mean equal to the variance. The z distribution with bias potential $W_i(z)$, as estimated from a finite time simulation with a total number of points M_i, is $p_i^{est}(z)\Delta z = \langle H_i(z)\rangle / M_i$. The exact nonbiased z distribution, $p_0(z)$, is related to the exact biased z distribution $p_i(z)$ via

$\ln(p_i/p_0) = (\Delta F - W_i)/kT$ or

$$p_0(z) = \exp(W_i)\frac{Z_i}{Z_0}p_i(z)$$

Here Z_i and Z_0 are the corresponding partition functions while $\Delta F = F_{ins}(z)$ is the free energy difference between the two systems. The constructed estimate for nonbiased z distribution within the SCH method is

$$p_0^{est}(z) = \sum_{i=1}^{n} w_i(z)\exp(W_i/kT)\frac{Z_i}{Z_0}p_i^{est}(z) \qquad (19)$$

where $w_i(z)$ is a weight function such that $\sum w_i(z) = 1$ and the variance of $p_0^{est}(z)$ is minimal. This leads to

$$p_0^{est}(z) = \frac{\sum_{i=1}^{n} H_i(z)}{\sum_{i=1}^{n}\exp(-W_i/kT)M_iZ_0/Z_i} \qquad (20)$$

where the values of Z_i are determined from the self-consistent solution of a set of n non linear equations obtained from eq 20 upon substituting $Z_i = \int dzZ_0p_0^{est}(z)\exp(-W_i/kT)$

$$Z_i = \int dz\exp(-W_i/kT)\frac{\sum_{j=1}^{n} H_j(z)}{\sum_{k=1}^{n}\exp(-W_k/kT)M_k/Z_k} \qquad (21)$$

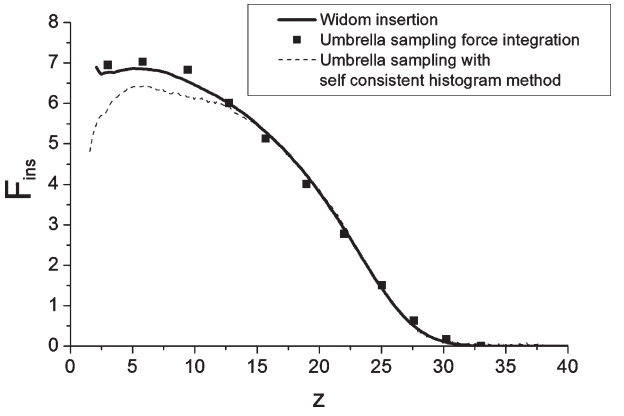

Figure 3. Comparison between the insertion free energy, F_{ins}, as obtained by force integration, the self-consistent histogram method and the Widom insertion method for $R_p = 1.5$, $N = 50$, and $d = 3$.

The equations determine the Z_i/Z_1 ratios and it thus necessary to arbitrarily fix $Z_1 = 1$. The solution is obtained iteratively

$$Z_i^{(j)} = \int dz\exp(-W_i/kT)\frac{\sum_{j=1}^{n} H_j(z)}{\sum_{k=1}^{n}\exp(-W_k/kT)M_k/Z_k^{(j-1)}} \qquad (22)$$

where $Z_i^{(j)}$ is value of Z_i in the jth iteration and the initial values $Z_i^{(0)} = 1$ were chosen for all i. To ensure a unique solution Z_1, which corresponds to largest z_i, was fixed at $Z_1^{(j)} = 1$ for all j values . The convergence criterion utilizes

$$\Delta(j) = \sum_i (\ln Z_i^{(j)} - \ln Z_i^{(j-1)})^2 \qquad (23)$$

and the iteration is stopped at j_{max} corresponding to $\Delta(j_{max}) \leq 10^{-3}$. A solution usually requires less than 20 iterations. $p_0^{est}(z)$ is than calculated using eq 20 with $Z_i^{(j_{max})}$ replacing Z_i and the corresponding $F_{ins}(z)$ is obtained from $F_{ins}(z) = -kT\ln p_0^{est}(z)$.

Performance. Because of the limitations of the Widom insertion method, a comparison of the three methods for determining F_{ins} is only possible for small particles and to this end we have used $R_p = 1.5$. The Widom insertion method results were obtained using 240×10^6 MCS. The 11 points measured by the force integration method required 15×10^6 MCS per point and thus a total of 165×10^6 MCS. The SCH method required 40×10^6 MCS per point and thus a total of 440×10^6 MCS. The three method led to identical results in the outer range $12.5 \leq z \leq 40$ (Figure 3). The force integration and Widom insertion method also yielded indistinguishable results for the inner range $2.5 \leq z \leq 12.5$. In contrast, the SCH values in this range are lower. The deviation is small in the $5 \leq z \leq 12.5$ interval but the SCH results are significantly lower for $2.5 \leq z \leq 5$.

IV. Simulation Results

Our results fall into two groups: concentration profiles of brushes with inserted particles and insertion free energies in units of kT. The concentration profiles are presented in three forms: (i) Monomer density contours, $\phi = \phi(z,\rho)$ in a cylindrical coordinate system where z is the altitude and ρ is the distance from the z

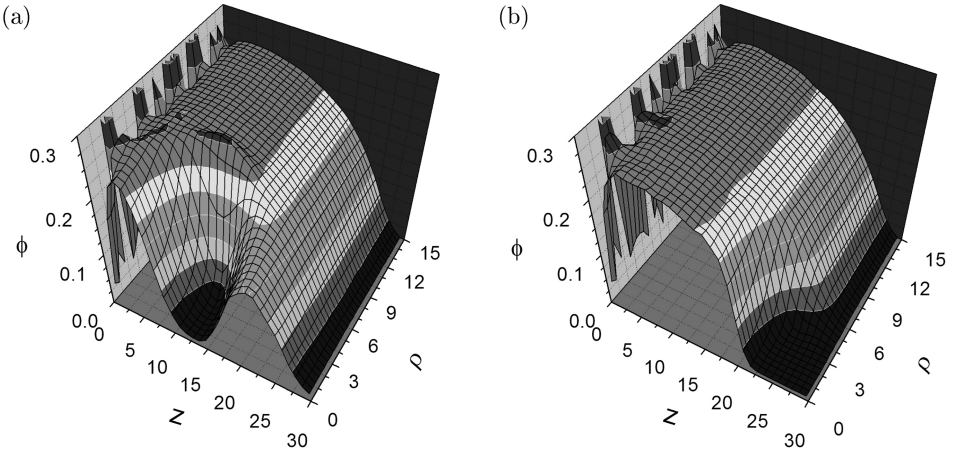

Figure 4. Monomer density contours, $\phi = \phi(z, \rho)$ for $R_p = 4$ and $d = 3$ (a) for $z_{eq} = 12.2$ corresponding to $z_i^0 = 7$ and (b) $z_{eq} = 24.2$ corresponding to $z_i^0 = 16$.

axis passing through the center of the particle (Figure 4). In this presentation $\phi(z,\rho)$ is an azimuthal average. This is the most complete data presentation. It gives an overall view but does not allow for quantitative comparison between features. This global view is thus supplemented by two cross sections. (ii) Vertical $\phi = \phi(z)$ plots specify ϕ at different z at horizontal distances $\rho = 0, 4, 8$ from the z axis passing through the center of the particle (Figure 5). These correspond to sections of $\phi = \phi(z,\rho)$ along the selected ρ values permitting detailed comparison between them. This plot is physically interesting since it concerns the reaction coordinate of the particle insertion. However, this form is not ideal for investigating the particle induced perturbation because $\phi = \phi(z)$ varies even in the absence of particle and the ϕ values in the vicinity of the particle reflect the superposition of the unperturbed brush $\phi = \phi(z)$ with the effects induced by the particle. (iii) To gain information on depletion effects it is thus advantageous to utilize "equatorial" $\phi = \phi(r)$ plots in spherical coordinate system whose origin is at the center of the particle. These characterize the azimuthal average of ϕ in a narrow angular interval around the equatorial plan of the particle as a function of r, the radial distance from the center of the particle (Figure 6). In particular, upon denoting the angle between the r vector and the normal to the grafting surface by Ω, we divide the $\Omega \in [0,\pi]$ range into 100 bins and plot the average values of the two bins around $\Omega = \pi/2$, i.e., the bins corresponding to the interval $1.54 < \Omega < 1.60$. In this cross section, the unperturbed brush is translationally uniform and the r dependence of $\phi(r)$ results from the perturbation induced by the particle. In particular, it is possible to clearly characterize the relaxation of $\phi(r)$ toward the unperturbed region at the edge of the simulation box.

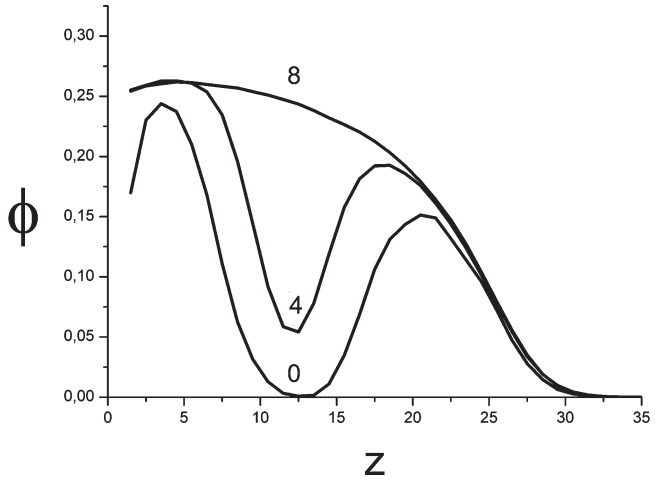

Figure 5. Vertical $\phi = \phi(z)$ plots along the z axis at distances $\rho = 0, 4, 8$ from the z axis passing through the center of the particle with $R_p = 4$, $z_{eq} = 12.2$ corresponding to $z_i^0 = 7$ for a brush with $N = 50$ and $d = 3$. For $\rho = 8$, the concentration profile is indistinguishable from that of a bare brush.

All plots suggest that the perturbation of the ϕ profile due to the particle is short ranged and that ϕ decays toward its unperturbed values within a short distance from the surface of the particle. The corresponding decay length increases with z but remains of order a. Qualitatively similar picture emerges from the $\phi = \phi(z,\rho)$ and $\phi = \phi(z,\rho = 0)$ plots presented by Milchev et al.[2] The equatorial views (Figure 6) reveal, in addition, the occurrence of two scenarios: The depletion layer at the surface of deeply inserted particles does not relax monotonically to the unperturbed brush values. Instead, $\phi(r)$ exhibits a weak maximum, within a distance $\approx a$ to $\approx 2a$ from the surface of the particle, before decaying to the unperturbed brush value. On the other hand, shallow insertions are associated with "pure" depletion, i.e, a monotonic variation of $\phi(r)$. This feature may be due to the immobility of the chain anchors in our simulation. In particular, it may arise because the lateral displacement of the brush monomers from the volume occupied by the particle is limited in range because the grafting sites in the simulation are fixed.

The free energy curves obtained (Figure 7) reveal two qualitative features: One, the insertion free energy penalty F_{ins} grows as z decreases. In other words, F_{ins} grows with the depth of insertion and the corresponding increase in $\phi(z)$ of the unperturbed brush encountered by the particle. F_{ins} also increases with the particle radius R_p. Both features were observed in earlier simulations of Jönsson and Johansson[19] and of Milchev et al.[2] For sufficiently low R_p we also observe a wall effect due to the depletion layer at the grafting surface. This gives rise to lower F_{ins} at $z < z_{max}$. Within the umbrella sampling measurements the depletion effect is signaled by the form of the z-histograms. For $z \gg z_{max}$ the z-histograms exhibit a maximum displaced outward with respect to z_{0i}. In contrast, in the interior region the z of the maximum is shifted toward the wall. The decrease in F_{ins} is likewise evident in the Widom insertion method. This feature was also observed in the simulations of Jönsson and Johansson.[19]

The qualitative features of F_{ins} (Figure 7) do not allow to identify its physical origin because all versions of F_{ins}, as summarized in section II, exhibit identical trends. To explore this issue we recall that F_{ins} of solutions assumes two limiting forms: For $R_p \gg \xi$ the osmotic penalty $F_{ins}/kT \approx (R/\xi)^3$ dominates while for $R_p \ll \xi$ the de Gennes form $F_{ins}/kT \approx (R/\xi)^{4/3}$ is operative. Noting that the minimal blob size in our simulations is roughly $d = 3$ we thus expect to distinguish between particles with $R_p < 3$ such that $R_p < \xi(z)$ for all z, and particles with $R_p > 3$ such that $R_p > \xi(z)$ for sufficiently deep insertions. These observations suggest plotting F_{ins}/R_p^3 and $F_{ins}/R_p^{4/3}$ vs ϕ of the unperturbed brush

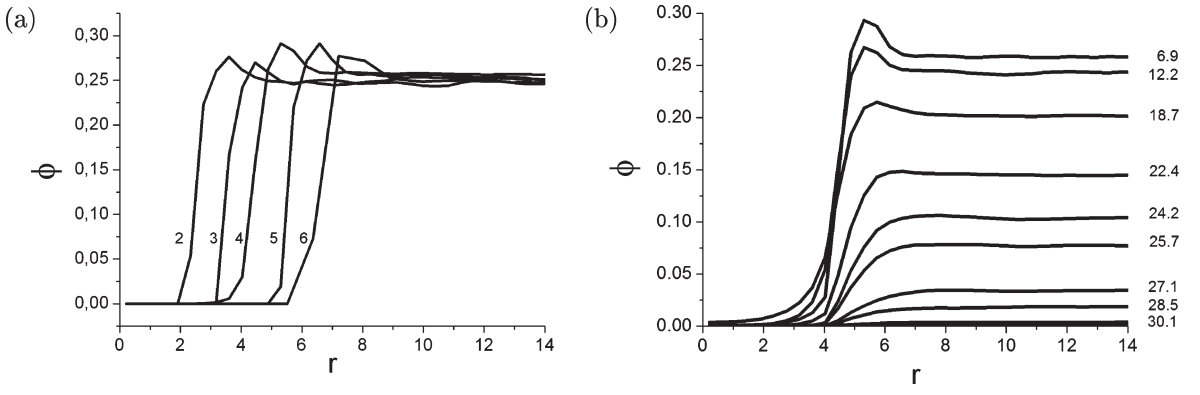

Figure 6. Equatorial $\phi = \phi(r)$, in the equatorial plane of the particle (a) as a function of r the radial distance from the center of a particle for particles of radius $R_p = 2, 3, 4, 5, 6$ at $z_e q = 10$ (b) for different z_{eq} for a particle of $R_p = 4$. In both cases $N = 50$ and $d = 3$.

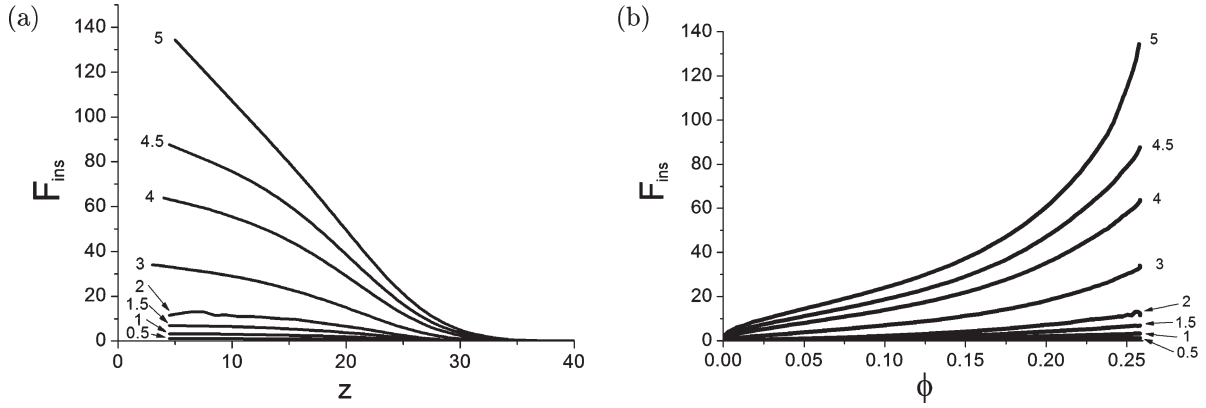

Figure 7. Insertion free energy F_{ins} as a function of (a) the altitude z and (b) monomer volume fraction ϕ for $0.5 \leq R_p \leq 5$, $N = 50$ $d = 3$.

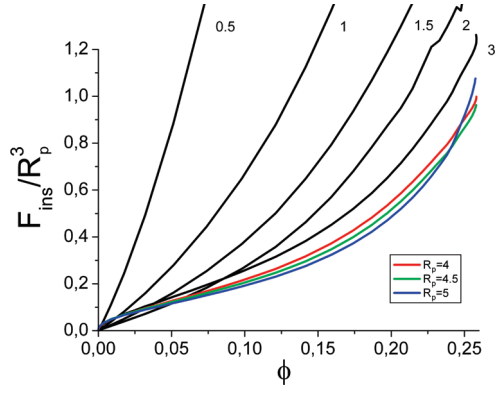

Figure 8. F_{ins}/R_p^3 vs ϕ plots for for $0.5 \leq R_p \leq 5$, $N = 50$, and $d = 3$.

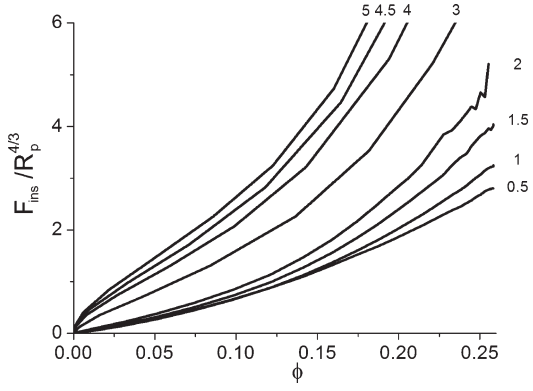

Figure 9. $F_{ins}/R_p^{4/3}$ vs ϕ plots for $0.5 \leq R_p \leq 5$, $N = 50$, and $d = 3$.

i.e. ϕ corresponds to the unperturbed brush $\phi(z)$ value at the z specifying the altitude of the center of the inserted particle (Figures 8 and 9). The first plot should collapse the data for the osmotic regime while the second is expected to do so if the de Gennes regime is realized. For our $\sigma = 1/d^2$ and the range of R_p explored we observe collapse of the F_{ins}/R_p^3 curves for $R_p \geq 3$. The ϕ range of the collapse increases with R_p. For $4 \leq R_p \leq 5$ the curves collapse over the whole ϕ range while for $R_p = 3$ only the low ϕ region is concerned. No collapse is discernible for $0.5 \leq R_p \leq 2$. In contrast, comparison of $F_{ins}/R_p^{4/3}$ vs ϕ and F_{ins} vs ϕ plots does not reveal enhanced collapse of the curves in any R_p range. The excluded volume of the particle is actually larger than its geometric volume because the centers of the hard-core monomers are excluded from a shell of thickness 1/2 surrounding it. In the R_p range explored this a significant effect and it is thus of interest to consider similar plots upon replacing R_p by $\bar{R}_p = R_p + 1/2$. There is no marked collapse in the $F_{ins}/\bar{R}_p^{4/3}$ vs ϕ curves (Supporting Information, Figure 1). In contrast, the $F_{ins}/\bar{R}_p^3$ vs ϕ plot show significant improvement in the collapse of the $R_p \geq 3$ curves (Figure 10). As in the F_{ins}/R_p^3 plot, the $0.5 \leq R_p \leq 2$ curves are distinct from each other and from the $4 \leq R_p \leq 5$ curves over most of the ϕ range. On the other hand, the $4 \leq R_p \leq 5$ curves collapse onto a single curve. In addition, all curves overlap in the low ϕ range and the maximal deviation between the various curves at high ϕ is reduced.

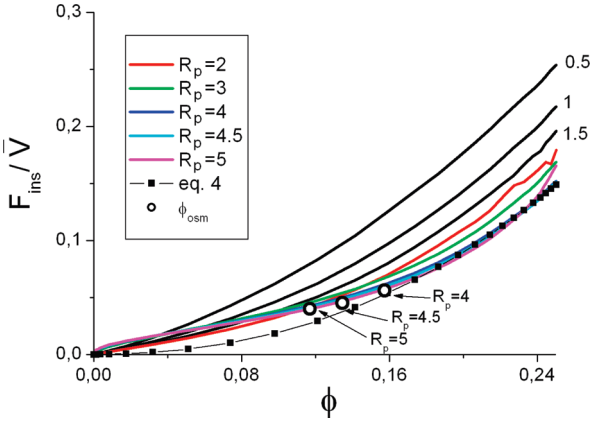

Figure 10. $F_{ins}/\bar{V}_p$ vs ϕ plots for $0.5 \leq R_p \leq 5$, $N = 50$, and $d = 3$ also showing the calculated Π using eq 4 with $A = 1.6$. The ○ represent ϕ_{osm} for the corresponding $\bar{R}_p$.

The $F_{ins}/R_p^{4/3}$ plot described above supports a negative conclusion: There is no evidence for the de Gennes regime in the parameter range we explored. The situation with regard to the osmotic regime is less clear-cut. The collapse of the large R_p curves in the $F_{ins}/\bar{R}_p^3$ plot is consistent with the occurrence of an osmotic regime. Further analysis is however needed because the collapse occurs over the whole ϕ range and not just for $R_p \gg \xi$. To explore this issue we first plot $F_{ins}\,(\xi/\bar{R}_p)^3$ vs ϕ (Figure 11). A regime with $F_{ins}/kT \approx (\bar{R}_p/\xi)^3$ should manifest itself by collapse onto a horizontal curve as is indeed observed for $3 \leq R_p \leq 5$ in the $0.12 \leq \phi \leq 0.25$ range. For this range $F_{ins}/kT \simeq 13.68(\bar{R}_p/\xi)^3$. Importantly, $F_{ins}/kT \approx (\bar{R}_p/\xi)^3$ underestimates the measured F_{ins} for $\phi < 0.1$. Whereas this last plot establishes the origin of F_{ins}/kT at the interior of the brush, it provides little insight on the low ϕ region where $\Pi \approx kT/\xi^3$ is not expected to hold. To explore this regime we utilize eq 4 since it specifies Π over the whole ϕ range. In particular, we plot $F_{ins}/\bar{V}_p$ vs ϕ where $\bar{V} = (4\pi/3)\bar{R}_p^3$ and fit the $3 \leq R_p \leq 5$ curves to eq 4 (Figure 10). The $0.17 \leq \phi \leq 0.25$ range of these curves can be fitted to $\Pi(\phi)$ as give by eq 4 using $\phi_{ex} = A\phi^*$ with $A = 1.6$ and with ϕ^* corresponding to our N. However, this fitted $\Pi(\phi)$ also underestimates $F_{ins}/\bar{V}_p$ for $\phi <$ 0.17. The comparison between $A = 1.6$ we find and $A = 0.69$

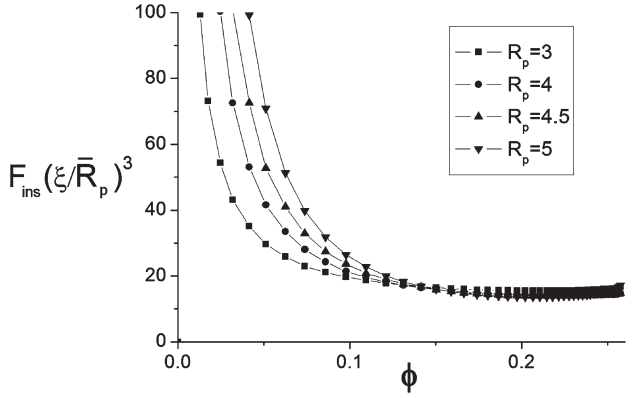

Figure 11. $F(\xi/\bar{R}_p)^3$ vs ϕ plots for $3 \le R_p \le 5$, $N = 50$, and $d = 3$.

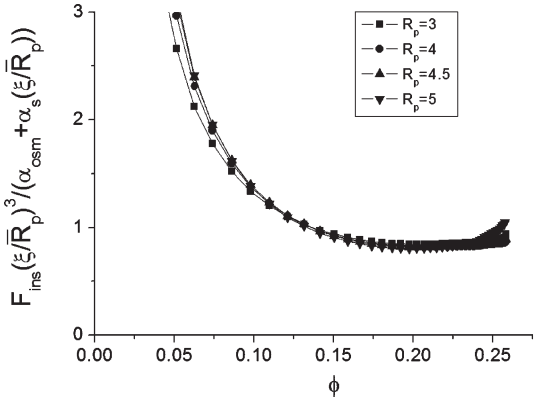

Figure 12. $F(\xi/\bar{R}_p)^3(\alpha_{osm} + \alpha_s(\xi/\bar{R}_p))$ vs ϕ plots for $3 \le R_p \le 5$, $N = 50$, $d = 3$, $\alpha_{osm} = 13.68$, and $\alpha_s = 5.22$.

corresponding to athermal solutions in the limit of $N \to \infty$ is not informative because scaling corrections[30] may play a role for the $N = 50$ chains we utilize. We finally add that ϕ_{osm} as specified by eq 9 provides a rough indicator for the onset of applicability of both $F_{ins}/kT \approx (\bar{R}_p/\xi)^3$ and eq 4 (Figure 10).

The evidence summarized above indicates that an osmotic regime $F_{ins}/kT \approx (R_p/\xi)^3$ occurs for deeply inserted $R_p \ge 3$. However, $F_{ins}/kT \approx (R_p/\xi)^3$ underestimates the measured F_{ins} of $R_p \ge 3$ at low ϕ and of $R_p < 3$ for all ϕ. Since we find no evidence for the occurrence of a de Gennes regime, the discussion of section suggests that the low ϕ range may reflect surface tension corrections, i.e.

$$F_{ins}/kT \approx \alpha_{osm}(R_p/\xi)^3 + \alpha_s(\xi/R_p)^2 \qquad (24)$$

where α_{osm} and α_s are the proportionality constants for the osmotic and surface terms. As we discussed earlier, Figure 11 yields $\alpha_{osm} = 13.68$. Using this value to fit the F_{ins} of $R_p = 5$ over the range $0.10 \le \phi \le 0.15$ leads to $\alpha_s = 5.22$. In turn, these values of α_{osm} and α_s allow to collapse the $R_p \ge 3$ curves in the plot of $F_{ins}(\xi/\bar{R}_p)^3/[13.68 + 5.22\,(\xi/\bar{R}_p)]$ vs ϕ (Figure 12). However, $F_{ins}/kT \approx 13.68\,(R_p/\xi)^3 + 5.22\,(\xi/R_p)^2$ underestimates the measured F_{ins} in the low ϕ range. This reflects a $\phi^{-\delta}$ dependence in the range $\phi < 0.1$ with a R_p dependent $\delta \simeq 1.46-1.65$ (Supporting Information). Altogether, these results suggest that the surface correction $\sim (\xi/R_p)^2$ contributes to F_{ins} though an additional $\phi^{-\delta}$ dependence, having no clear explanation in the results summarized in section II, plays an important role.

Milchev et al [2] concluded from their simulation results that $F \sim R_p^2$ occurs for shallow insertions while $F \sim R_p^3$ scaling characterize deeply inserted particles. With this in mind we plotted $F_{ins}/\bar{R}_p^2$ and $F_{ins}\,(\xi/\bar{R}_p)^2$ vs ϕ (Supporting Information). These plots did lead to an improved collapse with an overall reduction in the deviation between the curves. The $R_p = 1.5-2$ curves collapsed over the whole ϕ range while the $R_p = 4,4.5,5$ collapsed in the range $0 \le \phi \le 0.15$. The two groups do not lie however on the same master curve. Overall, these results do not fully support the conclusion that F_{ins}/R_p^2 and F_{ins}/R_p^3 scaling characterize the brush F_{ins} for shallow and deep insertions for all R_p values.

V. Discussion

Using Monte Carlo simulation with umbrella sampling we probed the interaction between a planar brush and spherical nonadsorbing particles. In our study the brush was swollen by athermal solvent and the radius of the hard-core particle was smaller than the height of the unperturbed brush, $R_p < h_0$. Our results concern two features. One is the particle induced perturbation of the monomer concentration profile. The second is the insertion free penalty F_{ins} incurred upon introducing the particle into the brush. Both features were studied as a function of R_p and the particle altitude z. With regard to the first issue we find that the perturbation is local and short ranged. Pure depletion characterizes shallow insertions while deep insertion gives rise to a depletion region followed by a maximum. Qualitatively, F_{ins} grows with ϕ and R_p. Accordingly F_{ins} increases with the depth of insertion so long as the particle does not experience the depletion layer at the grafting surface. Importantly, the brush $F_{ins}(z)$ is related to the bulk F_{ins} assuming that the particle encounters $\phi(z)$ of the unperturbed brush. Particles with $R_p \ge 3$ exhibit a clear osmotic regime where $F_{ins}(z) \approx \Pi(z)V_p \sim R_p^3$. This occurs for relatively deep insertions. The osmotic penalty underestimates F_{ins} at shallower insertions where a surface tension correction of the form $\alpha_s\,(\xi/R_p)^2$ plays a role. In this range we note an additional a $\phi^{-\delta}$ dependence with a R_p-dependent $\delta \simeq 1.46-1.65$. F_{ins} of smaller particles exhibit neither the $\sim R_p^3$ scaling of the osmotic penalty nor the $\sim R_p^{4/3}$ scaling expected for the de Gennes regime, $F_{ins}/kT \approx (R_p/\xi)^{4/3}$. In this R_p range our shallow insertion data exhibits $\sim R_p^2$ behavior though the curves in the F/R_p^2 vs ϕ plots form distinctive groups with different collapse regions. Similar trends were observed, with certain differences, in earlier studies by Jönsson and Johansson[19] and by Milchev et al.[2] In comparing the results of the various simulations, one should note differences in modeling and methods. Jönsson and Johansson utilized a lattice model and the Widom insertion method on relatively sparse brushes. Milchev et al. considered relatively dense brushes using finitely extensible nonlinear elastic potential for modeling the chain, a Morse potential to describe the interactions and the "particle inflation" method, a generalization of the Widom insertion method.

The insertive regime imposes $R_p \ll h_0 \approx N(a^2/\Sigma)^{1/3}$. Since N also controls the onset of chain overlap, increasing N will allow to investigate a wider range of R_p and Σ. In turn, this will enable to better explore the $R_p \ll \xi$ and $R_p \gg \xi$ limits while maintaining $a \ll R_p \ll h_0$. The use of higher N also incurs a computational price due to longer relaxations times. It is nevertheless desirable future direction in order to better explore the asymptotic behavior of F_{ins} and especially the de Gennes regime. Whereas our results support the occurrence of an osmotic regime $F_{ins}/kT \approx \alpha_{osm}\,(R_p/\xi)^3$ they do not resolve a question concerning the numerical value of α_{osm}. SCF theory suggests that the brush F_{ins}/kT should indeed scale as $\sim (R_p/\xi)^3$ but that α_{osm} should be larger than the corresponding bulk value, α_{osm}^{bulk} because the insertion penalty in the brush reflects a contribution due to the stretched configurations of the chains. To resolve this issue it is necessary to characterize F_{ins} into a bulk semidilute solution of free chains simulated using an identical polymer model. This, in turn, may be accomplished by simulations using the "particle inflation" method of Milchev et al.[2] To resolve the surface tension

contribution to F_{ins}, it is of of interest to determine the osmotic pressure of the simulated semidilute solution using, for example, the virial theorem.[48]

Our results concerned athermal solvents and nonadsorbing particles. The effect of solvent quality and particle−polymer attraction is yet to be systematically studied though exploratory results were reported by Jönsson and Johansson[19] and by Milchev et al.[2] Clearly, some results will be modified. The ϕ dependence of $\Pi(\phi)$ is expected to vary with the solvent quality and the "depletion" surface tension, $\gamma \approx kT/\xi^2$, may be modified by particle-polymer attraction. Other, more qualitative conclusions are likely to be less sensitive to the parameters of the system. One such conclusion is the very existence of an insertive regime, $R \ll h_0$, such that (i) the insertion induced perturbation of the brush structure is short ranged, (ii) the brush $F_{ins}(z)$ is largely determined by the unperturbed $\phi(z)$, and (iii) the brush $F_{ins}(z)$ is proportional to the corresponding bulk F_{ins} for $\phi = \phi(z)$. In turn, the occurrence of the insertive regime is of interest for formulating simple analytical models of the interactions between brushes and colloidal particles in general and between PEG brushes and proteins in particular.

Acknowledgment. We thank Professor A. R. Khokhlov for his encouragement and support. A.E. and V.E. acknowledge financial support of the Russian Foundation for Basic Research (project 09-03-01124-a) and Federal Agency for Science and Innovations of the Russian Federation (contract 2009-1.5-508-008-024) as well as by the international relations department of the CEA and the hospitality of SPrAM (CEA-Grenoble).

Supporting Information Available: Figures showing plots of $F_{ins}/\bar{R}_p{}^{4/3}$ vs ϕ, $\ln F_{ins}(\xi/\bar{R}_p)^3/[13.68 + 5.22(\xi/\bar{R}_p)]$ vs $\ln \phi$, $F_{ins}(\xi/\bar{R}_p)^2$ vs ϕ, and $F_{ins}/\bar{R}_p{}^2$ vs ϕ. This material is available free of charge via the Internet at http://pubs.acs.org.

References and Notes

(1) (a) Kim, J. U.; O'Shaughnessy, B. *Phys. Rev. Lett.* **2002**, *89*, 238301. (b) Kim, J. U.; O'Shaughnessy, B. *Macromolecules* **2006**, *39*, 413.
(2) Milchev, A.; Dimitrov, D. I.; Binder, K. *Polymer* **2008**, *49*, 3611.
(3) Jeon, S. I.; Lee, I.; Andrade, J. H.; de Gennes, P. G. *J. Colloid Interface Sci.* **1991**, *142*, 149.
(4) Szleifer, I. *Biophys. J.* **1997**, *72*, 595.
(5) Halperin, A. *Langmuir* **1999**, *15*, 2525.
(6) Currie, E. P. K.; Van der Gucht, J.; Borisov, O. V.; Cohen Stuart, M. A. *Pure Appl. Chem.* **1999**, *71*, 1227.
(7) Steels, B. M.; Koska, J.; Haynes, C. A. *J. Chromatogr B* **2000**, *41*, 743.
(8) Halperin, A.; Fragneto, G.; Schollier, A.; Sferrazza, M. *Langmuir* **2007**, *23*, 10603.
(9) Elbert, D. L.; Hubbell, J. A. *Annu. Rev. Mater. Sci.* **1996**, *26*, 365.
(10) *Poly(Ethylene Glycol) Chemistry: Biotechnical and Biomedical Applications*; Harris, J. M., Ed.; Plenum Press: New York, 1992.
(11) Lee, J. H.; Lee, H. B.; Andrade, J. D. *Prog. Polym. Sci.* **1995**, *20*, 1043.
(12) Goddard, J. M.; Hotchkiss, J. H. *Prog. Polym. Sci.* **2007**, *32*, 698.
(13) Currie, E. P. K.; Norde, W.; Cohen Stuart, M. A. *Adv. Colloid Sci.* **2003**, *100−102*, 205.
(14) Yang, J.; Yamato, M.; Okano, T. *MRS Bull.* **2005**, *30*, 189.
(15) Kanazawa, H.; Matsushima, Y.; Okano, T. *Adv. Chromatography* **2001**, *41*, 311.
(16) Harris, J. M.; Chess, R. *Nature Rev Drug Discovery* **2003**, *2*, 214.
(17) *Liposomes Rational Design*; Janoff, A. S., Ed.; Marcel Dekker: New York, 1998.
(18) Halperin, A.; Kröger, M. *Langmuir* **2009**, *25*, 11621.
(19) Jönsson, M.; Johansson, H.-O. *Colloids Surf. B* **2004**, *37*, 71.
(20) Louis, A. A.; Bolhuis, P. G.; Meijer, E. J.; Hansen, J. P. *J. Chem. Phys.* **2002**, *116*, 10547.
(21) de Gennes, P.-G. *Scaling Concepts in Polymer Physics*; Cornell, University Press: Ithaca, NY, 1979.
(22) Grosberg, A.Yu.; Khokhlov, A. R. *Statistical Physics of Macromolecules*; American Institute of Physics: New York, 1994.
(23) de Gennes, P. G. *C.R. Acad. Sci.Paris, Ser. B* **1979**, *288*, 359.
(24) Odijk, T. *Macromolecules* **1996**, *29*, 1842.
(25) Wang, S.; van Dijk, J. A. P. P.; Odijk, T.; Smit, J. A. M. *Biomacromolecules* **2001**, *2*, 1080.
(26) Hanke, A.; Eisenriegler, E.; Dietrich, S. *Phys. Rev. E* **1999**, *59*, 6853.
(27) Sear, R. P. *Phys. Rev. E* **1997**, *56*, 4463.
(28) Fleer, G. J.; Skvortsov, A. M.; Elbert, R. T. *Macromol. Theory Simul.* **2007**, *17*, 531.
(29) Schäfer, L. *Excluded Volume Effects in Polymer Solutions* Springer-Verlag: Berlin, 1999
(30) Pelissetto, A. *J. Chem. Phys.* **2008**, *129*, 044901.
(31) Milner, S. T. *Science* **1991**, *251*, 907.
(32) Zhulina, E. B.; Borisov, O. V.; Priamitsyn, V. A. *J. Collid Interface Sci.* **1990**, *137*, 495.
(33) Lai, P. Y.; Zhulina, E. B. *J. Phys. II Fr.* **1992**, *2*, 547.
(34) Wittmer, J.; Johner, A.; Joanny, J. F.; Binder, K. *J. Chem. Phys.* **1994**, *101*, 4379.
(35) Milner, S. T.; Witten, T. A.; Cates, M. E. *Macromolecules* **1988**, *21*, 2610.
(36) For the normalized variables $\tilde{z} = z/(N\sigma^{1/3})$ and $\tilde{\phi} = \phi/\sigma^{2/3}$ the concentration profile is

$$\tilde{\phi}(\tilde{z}) = \frac{3}{2\tilde{H}_0}\left(1 - \frac{\tilde{z}^2}{\tilde{H}_0^2}\right)$$

where

$$\tilde{H}_0 = \left(\frac{8}{\pi^2}\right)^{1/3}\left(\frac{2\pi a^2}{3}\right)^{1/3}$$

(37) Lai, P.-Y.; Binder, K. *J. Chem. Phys.* **1991**, *95*, 9288.
(38) Rapaport, D. C. *J. Chem. Phys.* **1979**, *71*, 3299.
(39) In general, for $\Delta U > 0$ a random number $t \epsilon [0,1]$ is generated and the move is accepted if $t < \exp(-\Delta U)$. For hard-core interactions this leads to a simplified procedure since ΔU can only assume two values, 0 and ∞. $\Delta U = \infty$ gives rise to $t > \exp(-\Delta U) = 0$ while $\Delta U = 0$ leads to $t < \exp(-\Delta U) = 1$
(40) Metropolis, N.; Rosenbluth, A. W.; Rosenbluth, M. N.; Teller, A. H.; Teller, E. *J. Chem. Phys.* **1953**, *21*, 1087.
(41) The simulation in ref 37 utilized the bond fluctuation model (BFM) where the polymer is inscribed on a lattice, in contrast to our off-lattice model. Within this approach a monomer can occupy eight sites on simple cubic lattice with a lattice constant a. To confront the BFM results with ours it is necessary to identify the effective monomer size and the effective bond length in the BFM model where the allowed range of monomer−monomer distances varies between $2a$ and $10^{1/2}a$. To this end note that within the Alexander model the free energy per chain in a brush, allowing for a monomer diameter a and a different bond length b, is

$$\frac{F}{kT} \approx \frac{h^2}{Nb^2} + \frac{vN^2}{\Sigma h}$$

where $v \approx a^3$ is virial coefficient in an athermal solvent and h is the brush height . The corresponding equilibrium brush height is thus $h_0/a = (v/a^3)^{1/3}\,(b/a)^{2/3}\,N(a^2/\Sigma)^{1/3}$ and the equilibrium monomer volume fraction is $\phi_0 = (v/a^3)^{-1/3}\,(b/a)^{-2/3}\,(a^2/\Sigma)^{2/3}$. To compare the two simulation methods to we plotted $\phi(z)(\Sigma/a^2)^{2/3}$ vs $z/N(a^2/\Sigma)^{1/3}a$ and fitted the BFM results to ours, using least-squares method, by scaling the BFM results by $\phi_0^{BFM}/\phi_0 = 0.9$ and $h_0^{BFM}/h_0 = 2.25$. Since $\phi_0^{BFM}/\phi_0 = (b_{BFM}/b)^{-2/3}\,(a_{BFM}/a)^2$ and $h_0^{BFM}/h_0 = (b_{BFM}/b)^{2/3}$ (a_{BFM}/a) this suggests $a_{BFM}/a = 1.265$ and $b_{BFM}/b = 2.37$.
(42) Widom, B. *J. Chem. Phys.* **1963**, *39*, 2808.
(43) Frenkel, D.; Smit, B. *Understanding Molecular Simulation. From Algorithms to Applications*, 2nd ed.; Academic Press: London, 2002.
(44) Torrie, G. M.; Valleau, J. P. *J. Comput. Phys.* **1977**, *23*, 187.
(45) Leach, A. R. *Molecular Modeling Principles and Applications*; Longman Essex, 1996.
(46) Ferrenberg, A. M.; Swendsen, R. H. *Phys. Rev. Lett.* **1989**, *63*, 1195.
(47) The insertion free energy is $F_{ins} = F(N+1,V,T) - F(N,V,T) = -k_BT\,\ln(Q_{N+1}/Q_N)$ where $F(N,V,T) = -k_BT\,\ln Q_N$ is the free energy of a ensemble with N particles, $F(N+1,V,T)$ is the free energy of the ensemble with the added particle and Q is the corresponding classical partition function. The excess free energy of insertion is $F_{ex} = -k_BT\,\ln \int ds_{N+1}\,\langle \exp(-\beta\Delta U)\rangle_N$ where $\Delta U \equiv U(s^{N+1}) - U(s^N)$ is the change of energy associated with the insertion and $\langle ... \rangle_N$ denotes the canonical ensemble average over the configuration space of an equilibrated brush containing no particles. For hard-core interactions $p_{ins} = \int ds_{N+1}\,\langle \exp(-\beta\Delta U)\rangle_N$ is the probability of insertion a particle without incurring an overlap with a monomer or a bond.
(48) Milchev, A.; Binder, K. *Macromol. Theory Simul.* **1994**, *3*, 915.